Roles of Subcellular Na$^+$ Channel Distributions in the Mechanism of Cardiac Conduction

Kunichika Tsumoto,[†][*] Takashi Ashihara,[‡] Ryo Haraguchi,[§] Kazuo Nakazawa,[§] and Yoshihisa Kurachi[¶][†][*]

[†]The Center for Advanced Medical Engineering and Informatics, Osaka University and [¶]Division of Molecular and Cellular Pharmacology, Department of Pharmacology, Graduate School of Medicine, Osaka University, Osaka, Japan; [‡]Department of Cardiovascular and Respiratory Medicine, Heart Rhythm Center, Shiga University of Medical Science, Shiga, Japan; and [§]Laboratory of Biomedical Science and Information Management, Research Institute, National Cerebral and Cardiovascular Center, Osaka, Japan

ABSTRACTS   The gap junction and voltage-gated Na$^+$ channel play an important role in the action potential propagation. The purpose of this study was to elucidate the roles of subcellular Na$^+$ channel distribution in action potential propagation. To achieve this, we constructed the myocardial strand model, which can calculate the current via intercellular cleft (electric-field mechanism) together with gap-junctional current (gap-junctional mechanism). We conducted simulations of action potential propagation in a myofiber model where cardiomyocytes were electrically coupled with gap junctions alone or with both the gap junctions and the electric field mechanism. Then we found that the action potential propagation was greatly affected by the subcellular distribution of Na$^+$ channels in the presence of the electric field mechanism. The presence of Na$^+$ channels in the lateral membrane was important to ensure the stability of propagation under conditions of reduced gap-junctional coupling. In the poorly coupled tissue with sufficient Na$^+$ channels in the lateral membrane, the slowing of action potential propagation resulted from the periodic and intermittent dysfunction of the electric field mechanism. The changes in the subcellular Na$^+$ channel distribution might be in part responsible for the homeostatic excitation propagation in the diseased heart.

INTRODUCTION

The coordinated propagation of electrical excitation is crucial for normal contractile function in the heart. The abnormalities in action potential (AP) propagation, such as slow conduction and unidirectional block that underlie conduction heterogeneities in cardiac tissue, are involved in cardiac arrhythmias.

The electrical excitation in cardiac myocytes is known to propagate from cell to cell through gap junctions between adjacent cells. The electrical conductance between cells can be changed by altering the gap-junctional conductance (G_g) due to the effect of drugs [1,2], myocardial ischemia [3,4], or by changing the expression of connexins [5,6] (gap-junction channel-forming proteins [7]). In fact, gap-junctional coupling is attenuated by an alteration of the pattern of connexin expression in the cell membrane under various pathophysiological conditions [8–10]. Experimental [11] and numerical [12,13] studies have shown that a reduced gap-junctional coupling leads to the slowing of conduction velocity (CV). However, in several studies using genetically engineered murine models such as connexin (Cx) 43 knockout mice, Cx43 heterozygotes, and cardiac-restricted Cx43 conditional knockout (CKO) mice [14–17],

it has been pointed out that the relationship between gap-junctional coupling and CV might be complex. In particular, despite the fact that the G_g in Cx43 CKO mice was decreased to <10% of the one in wild-type mice [17], the actual CV in the Cx43 CKO mice measured by Gutstein et al. [16] was as much as 50% of that in wild-type.

Such experimental observations are not fully reproduced in numerical models of AP propagation via gap junctions [12,13]. Therefore, it is probable that other propagating mechanisms contribute to AP propagation. In previous theoretical studies [18,19], a propagating mechanism responsible for a large negative extracellular potential in the narrow cleft space of intercellular junctions, the so-called electric field (EF) mechanism, was proposed as an alternative to the gap-junctional mechanism. The EF mechanism postulates that during AP propagation from cell to cell, the large inward Na$^+$ channel (NaCh) current on the proximal side of an intercellular cleft generates the large negative extracellular potential within the cleft, which, in turn, activates the inward NaCh current in the adjacent cell on the distal side of the cleft.

Voltage-gated NaCh current is responsible for the onset of AP and the AP propagation in the myocardium, and therefore, modulating the NaCh function has an important impact on membrane excitability. It has been reported that cardiac-type NaChs together with gap junctions are intensively expressed at junctional membrane (JM) facing intercellular cleft (i.e., intercalated disk), but are also slightly expressed in the lateral part of the cell membrane (LM) of the myocyte [20–23]. The distribution of NaChs may change under pathophysiological cardiac remodeling [23].

Editor: Andrew McCulloch.

A recent simulation study (24) incorporating both the gap-junctional mechanism and the EF mechanism revealed that the localization of NaChs at the JM could maintain AP propagation even if gap-junctional coupling was greatly reduced. Nevertheless, the physiological significance of the distribution of NaChs at LM on AP propagation is not yet fully understood.

In this study, we conducted simulations of AP propagation along a myocardial fiber electrically coupled with gap-junctional mechanism alone or with both the gap-junctional mechanism and the EF mechanism at each cell junction. The purpose of this study was to elucidate how the NaChs, expressed at both JM and LM, play roles in AP propagation. In this article, we confirmed that both the gap-junctional mechanism and the EF mechanism contribute to the AP propagation in ventricles as reported previously (18,19,24), and showed that the property of AP propagation is greatly changed by the different subcellular distribution of NaChs if the EF mechanism is the case.

We found that the presence of NaChs in the LM was important to ensure the stability of AP propagation under conditions of decreased gap-junctional coupling, and that during the AP propagation in the poorly coupled tissue with sufficient NaChs in the LM, the slowing of AP propagation resulted from the periodic and intermittent dysfunction of the EF mechanism. In addition, without NaChs distribution to the LM, AP propagation based on the EF mechanism was unstable, and the morphology of the propagating AP was greatly affected, suggesting that changes in the subcellular NaCh distribution might be in part responsible for the homeostatic excitation propagation in the diseased heart.

METHODS

Myofiber model

To study the effect of subcellular distribution of NaChs on AP propagation, we used a one-dimensional myofiber consisting of serially arranged ventricular cells shown in Fig. 1 A. In this model, all cells had the same length (100 μm) and width (22 μm) (13), to prevent the effects of heterogeneity of cell size and shape on AP propagation (25).

The intercellular clefts facing at JMs were very narrow (5 ~25 nm) (5,7,26), and the resistance of the extracellular cleft space was thought to be higher than that of the bulk medium. Thus, an inward NaCh current generated at the JM induced a large negative extracellular potential within the narrow cleft space (18,19,24). We assumed that the adjacent cells are electrically coupled with the current through the gap junction at JM and with the change in the cleft potential (*cleft model*, Fig. 1 B). We also constructed a model coupled only with gap junctions (*noncleft model*, Fig. 1 C) to compare with the cleft model.

The whole cell membrane of each myocyte was divided into five segments; three segments of LM and two segments of JM (Fig. 1, B and C). In Fig. 1, B and C, the myoplasmic resistance (R_i) in between nodes in a myocyte was defined by

$$R_i = \rho_{myo} \cdot l_a / \pi r^2,$$

where ρ_{myo} is the myoplasmic resistivity (150 $\Omega \cdot$cm) (13), l_a is the length of the LM segment (33.3 μm), and r is the radius of the myocardial cell (11 μm). A value of 395 kΩ was chosen for the gap-junctional resistance (R_g) as the control value as it was identical to the myoplasmic resistance in an entire myocardial cell (13), i.e., the gap-junctional conductance (G_g) was 2.534 μS. The radial cleft resistance (R_j) was given by

$$R_j = \rho_{ext} / 8\pi w,$$

according to Katz (27), while the series axial resistance (R_d) was assumed to be

$$R_d = \rho_{ext} \cdot w / \pi r^2,$$

where ρ_{ext} is the extracellular resistivity (150 $\Omega \cdot$cm) (24), and w is the cleft width, which is the distance between the pre- and postjunctional
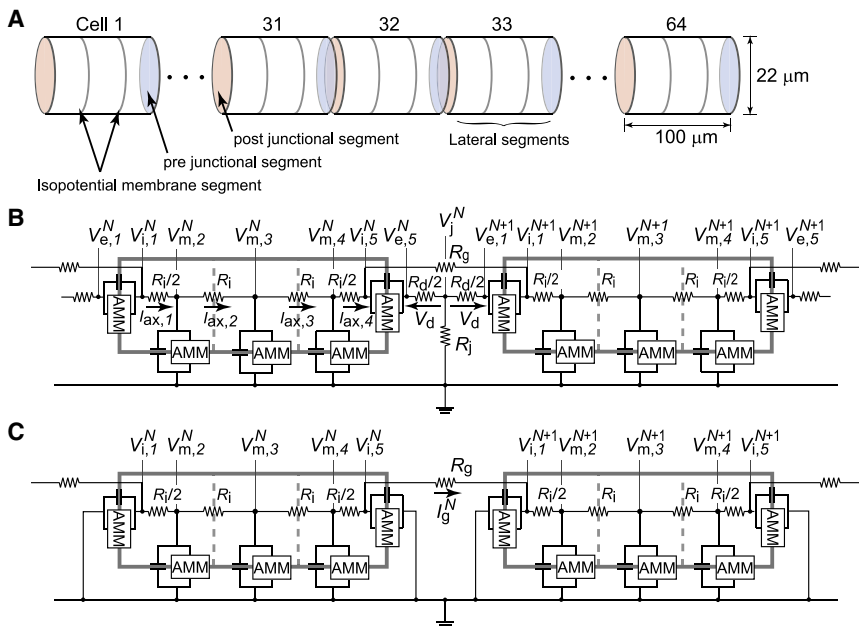

FIGURE 1 Schematic of strand model and equivalent circuits. (*A*) The strand model consists of myocardial cells with a cylindrical shape. The length and radius of the myocardial cell are 100 μm and 11 μm, respectively. (*B* and *C*) The equivalent circuit of the cleft and noncleft models, respectively. Each membrane segment is composed of an active membrane model (AMM) and a membrane capacitance. V_j^N represents extracellular cleft potential just after the Nth cell. The values $V_{m,n}^N$, $V_{i,n}^N$, and $V_{e,n}^N$ represent transmembrane, intracellular, and extracellular potentials, respectively, of nth segment of the Nth cell. The values $n = 1$ and 5 denote junctional segments, and $V_{m,n}^N = V_{i,n}^N - V_{e,n}^N$. The values R_g and R_j represent the gap-junctional resistance and the cleft resistance, respectively.

membranes (pre- and post-JMs). The cleft conductance (G_j) was given by

$$G_j = 1/R_j.$$

Frequently used abbreviations and acronyms are listed in Table 1.

Membrane model

Each segment of the cell membrane consisted of a membrane capacitance and an active membrane model (AMM) as shown in Fig. 1, B and C. The membrane dynamics was described with the AMM proposed by our group (28,29), in which the L-type calcium channel current and the values of the maximum conductance related to the potassium currents, I_{Kr}, I_{Ks}, I_{Kp}, and I_{to} were modified from the Luo-Rudy dynamic model (30,31) to reproduce intrinsic AP properties in the feline epicardial myocyte (32). Furthermore, the initial values of $[Na]_i$ and $[Na]_o$ were set to 12.1 and 140 mM, respectively, in this study to establish a more realistic situation (31). Specific parameters in the myofiber consisting of the AMM and initial conditions can be found in Table S1 in the Supporting Material.

The maximum conductance of NaChs per unit area was set to 16 mS/cm^2 and therefore the entire NaCh conductance of each cell corresponded to ~1.23 μS (30,31), which we defined as the control value (g_{Na}). This value is just a standard value (16 mS/cm^2) in the computer model, and this value might be larger or smaller in the pathological conditions. In this study, to investigate what effect the subcellular NaCh distribution had on AP propagation, we varied the g_{Na} in the range around the control value, and we used two conditions, i.e.,

1. All NaChs were distributed only in the JM and there were no NaChs along the LM.
2. NaChs were distributed to both JM and LM.

Throughout the article, the NaCh conductances of JM and LM were expressed as a percentage of the g_{Na}, i.e., %$g_{Na,JM}$ and %$g_{Na,LM}$, respectively. The myofiber model with 100%$g_{Na,JM}$ and 50%$g_{Na,LM}$, for instance, indicates that each cell had altogether an increased number (150%) of NaChs relative to the control case.

Numerical calculations

From the equivalent circuits in Fig. 1, B and C, we could derive a circuit equation (details of the derivation of the circuit equation are given in the

TABLE 1 Frequently used abbreviations and acronyms

Abbreviation	Definition
CV	Conduction velocity
Cx	Connexin
CKO	Conditional knockout
AP	Action potential
EF	Electrical field
NaCh	Na$^+$ channel
JM	Junctional membrane facing intracellular cleft
LM	Lateral part of the cell membrane
AMM	Active membrane model
g_{Na}	Control value of the entire NaCh conductance of each cell
%$g_{Na,JM}$	NaCh conductance of JM
%$g_{Na,LM}$	NaCh conductance of LM
%$g_{Na,JM+LM}$	Total NaCh conductance (%$g_{Na,JM}$+%$g_{Na,LM}$)
G_g	Gap-junctional conductance
G_j	Cleft conductance
I_g	Gap-junctional current
V_j	Cleft potential

Supporting Material). The transmembrane potential in each segment is represented by

$$C_m dV_{m,k}^N / dt + I_{ion}\left(V_{m,k}^N, t\right) = i_{m,k}^N$$

for $N = 1, ..., 64$, and $k = 1, ..., 5$, where C_m is the membrane capacitance with specific capacitance 1 μF/cm^2, I_{ion} (μA/μF) is the total ionic current in the AMM, and $i_{m,k}^N$ (μA/μF) is the transmembrane current. For an arbitrary time t, all the transmembrane currents, $i_{m,k}^N$, were obtained by solving the circuit equation with the transmembrane potentials, as an initial condition. Thereby, we could calculate all membrane potentials at time $t + \Delta t$ in each segment, where Δt corresponds to the time step in the Euler method. The time step, Δt, was fixed at the value of 0.5 μs to compensate for the reduced size of the discretized space and for the acute change in the membrane potential due to the occurrence of the cleft potential. Transmembrane stimuli with a basic cycle length of 400 ms were applied to the middle lateral segment of the cell located at the fiber end. Each transmembrane stimulus had duration of 0.5 ms and strength of 300 μA/cm^2, which was threefold higher than the diastolic threshold.

We defined the activation time of each cell as the time when the cell membrane depolarized and reached –30 mV from the resting potential. Then, the CV was calculated based on the activation times of the 21st and 42nd cells.

RESULTS

Effects of subcellular NaCh distribution on AP waveform

Fig. 2, A and B, shows examples of the APs observed in the middle LM segment of the 32nd cell in the noncleft and cleft models, respectively, assuming that NaChs are only localized at the pre- and post-JMs, i.e., 100%$g_{Na,JM}$ and 0%$g_{Na,LM}$. The noncleft model exhibited typical AP waveform for ventricular myocytes (Fig. 2 A). The AP in the cleft model, on the other hand, had smaller amplitude of phase-0 and a larger phase-2 dome (Fig. 2 B). Details on the phase-0 of the regional membrane potentials in each segment are shown in Fig. S1.

To investigate what effect the NaChs expressed in LM had on the AP waveforms, we further conducted simulations of AP propagation where NaChs were added to LM (Fig. 2 C). Then, we found that as the %$g_{Na,LM}$ increased step-by-step from 0% to 50% of the g_{Na}, the APs became similar to that in the noncleft model (compare to Fig. 2 A).

Modulations of CV by subcellular NaCh distribution

The relationships between CV and the total NaCh conductance (%$g_{Na,JM+LM}$ = %$g_{Na,JM}$ + %$g_{Na,LM}$) of the cell membrane in the noncleft and cleft models are shown in Fig. 3. This figure shows CV as a function of the %$g_{Na,JM+LM}$ when the %$g_{Na,LM}$ varied independently. Intriguingly, CV in the noncleft model (Fig. 3 A) was only determined by %$g_{Na,JM+LM}$ per cell, regardless of the subcellular NaCh distribution, whereas CV in the cleft model was largely influenced by both %$g_{Na,JM+LM}$ and %$g_{Na,LM}$. For instance, the noncleft model with 0%$g_{Na,LM}$ still maintained AP
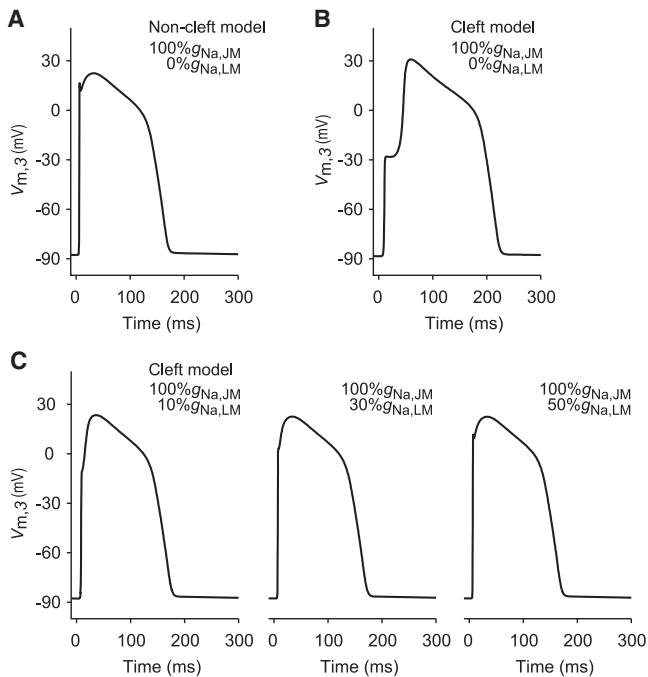
FIGURE 2 AP waveforms observed at a myocardial cell in the strand model. (*A* and *B*) AP waveforms in the noncleft and cleft models, respectively, in the case of 100%$g_{Na,JM}$ with 0%$g_{Na,LM}$. (*C*) AP waveforms in the cleft models where the NaChs are fixed at 100%$g_{Na,JM}$ with either 10%$g_{Na,LM}$ (*left*), 30%$g_{Na,LM}$ (*middle*), or 50%$g_{Na,LM}$ (*right*). In the strand model, we employed 2.534 μS for the gap-junctional conductance (G_g) and 0.25 μS for the cleft conductance (G_j). The values %$g_{Na,JM}$ and %$g_{Na,LM}$ indicate the NaCh conductances of junctional membrane (JM) and lateral membrane (LM), respectively.
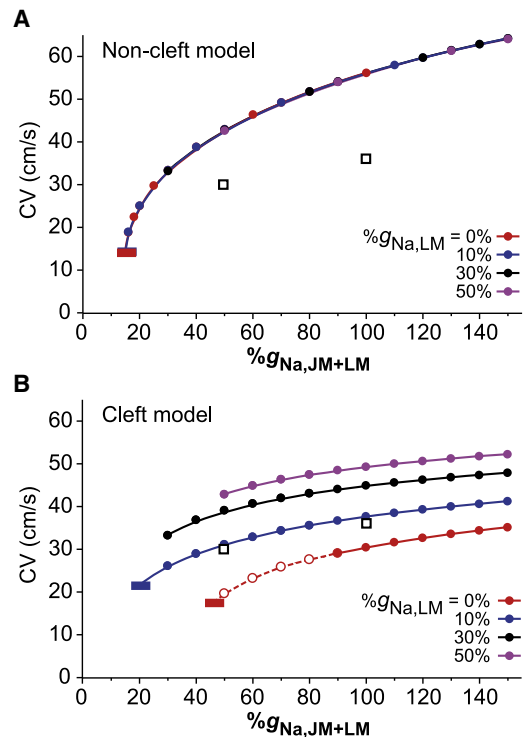

FIGURE 3 Conduction velocity (CV) as a function of total NaCh conductance (%$g_{Na,JM+LM}$) by changing NaCh distribution within the cell in the noncleft (*A*) and cleft (*B*) strand models. (*Dashed line* with the *open circles*) AP propagation with a triangular AP waveform. For purpose of comparison, experimental data (36) are plotted as open squares on panels *A* and *B*. (*Red* and *blue short horizontal bars*) Threshold for conduction block. In the models, we employed 2.534 μS for the gap-junctional conductance (G_g) and 0.25 μS for the cleft conductance (G_j).

propagation when %$g_{Na,JM+LM}$ (equal to %$g_{Na,JM}$ in this case) was reduced to 20%.

The critical CV just before conduction block was 14.0 cm/s in the case of 15%$g_{Na,JM+LM}$, corresponding to one-fourth of the CV in normal condition (56.2 cm/s with 100%$g_{Na,JM+LM}$). In contrast, the cleft model with 0%$g_{Na,LM}$ failed to propagate AP if %$g_{Na,JM+LM}$ (equal to %$g_{Na,JM}$) was reduced to <45% (Fig. 3 *B*), indicating that the safety of AP propagation was more sensitive to the changes in %$g_{Na,JM}$ than previously thought. Moreover, the addition of NaChs to LM (compare 0%$g_{Na,LM}$ and 10%$g_{Na,LM}$ in Fig. 3 *B*) led to an increase in CV and a decrease in the critical value of %$g_{Na,JM+LM}$ causing the conduction block. These results suggest that NaChs in the LM are important to keep the CV and to ensure the robustness of AP propagation in the reduced %$g_{Na,JM}$ condition.

Effects of cleft conductance change on AP propagation

We first confirmed a relationship between the CV and the G_j in the cleft model with the condition that NaChs are only localized in JM as reported previously (24). (Fig. 4 *A, left*). If the G_g was sufficiently large, the CV decreased monotonically as the G_j was reduced. By gradually reducing

the G_g, the relationship between the CV and the G_j shifted from the monophasic to biphasic behavior. An increase in the CV could be observed when the G_g was reduced to <10% of normal G_g (<0.253 μS) and the G_j was reduced to 0.5 μS, corresponding to the cleft width of ~30 nm. Further decrease in the G_j from 0.32 to 0.125 μS caused the reduction in CV from 14 to 7 cm/s. This result agreed well with the simulation results shown by Kucera et al. (24). In addition, we found that the AP resulted in an all-or-none repolarization and loss of the AP plateau or dome (Fig. 4 *A, right*) when the G_j was highly reduced (*dashed line* with *open circles* in Fig. 4 *A, left*). Thus, in the cleft model without NaChs in LM, an excessive reduction in the G_j resulted in the marked abbreviation of the AP duration as well as in the conduction block.

In another series of simulation, the number of NaChs in LM was gradually increased to examine what impact the NaChs in LM had on AP propagation when the G_j was varied. Fig. 4 *B* (*left*) shows CV as a function of G_j in the cleft model with 100%$g_{Na,JM}$ and 0%$g_{Na,LM}$. An almost constant CV was maintained when the G_g was relatively large and the G_j was decreased. Moreover, even if the G_j was 0.1 μS, corresponding to the cleft width of 6 nm, the
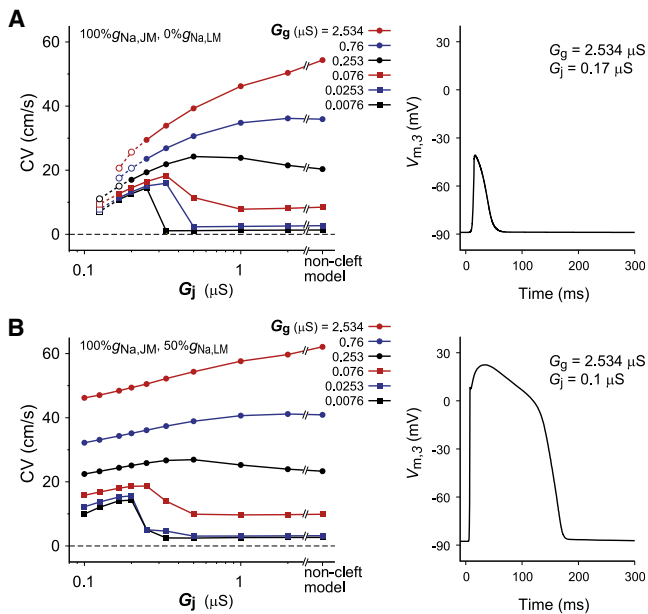
FIGURE 4 Conduction velocity (CV) as a function of cleft conductance (G_j) and AP waveforms in the case of $100\%g_{Na,JM}$ with $0\%g_{Na,LM}$ (A) and in the case of $100\%g_{Na,JM}$ with $50\%g_{Na,LM}$ (B) in the cleft model. AP waveform observed in the third segment of the 32nd cell where the cleft conductance (G_j) was set to 0.17 μS (cleft width, $w = 10$ nm) (A) and 0.1 μS ($w = 6$ nm) (B), respectively, and the gap-junctional conductance (G_g) was fixed at 2.534 μS.

propagation with the appropriate AP waveform could be maintained in the cleft model with $100\%g_{Na,JM}$ and $50\%g_{Na,LM}$ (Fig. 4 B, right). These results also suggest that the NaChs in LM increase the robustness of AP propagation under a variety of the G_j values.

AP propagation and gap-junctional conductance

Fig. 5 shows CV as a function of G_g between myocytes. As expected, the CV in the noncleft model gradually diminished with the decrease in the G_g independent of the subcellular NaCh distributions (Fig. 5 A). The critical value of G_g just before conduction block was ~0.3% of the normal G_g, at which the G_g was the same value as the intracellular axial conductance (2.534 μS); thus, the critical CV was 0.36 cm/s. Similar to the case in the noncleft model, a monotonic decrease in the CV was observed in the cleft model with $100\%g_{Na,JM}$ and $0\%g_{Na,LM}$ as the G_g was decreased. However, the slope of the CV-G_g curve of the $100\%g_{Na,JM}$ case in the cleft model was more gentle and the CV at low G_g was higher (~15 cm/s) than in the noncleft model (compare the solid red line and the gray dashed line in Fig. 5 B).

Furthermore, we confirmed that even in the absence of gap-junctional coupling, the CV was maintained at 14.7 cm/s. For comparison, we investigated the effect of the subcellular NaCh distribution on CV under the condition that the total number of NaChs per cell was kept constant at

the control value of g_{Na}. As shown in Fig. S2, not a decrease in $\%g_{Na,JM}$ but an increase in $\%g_{Na,LM}$ resulted in the steeper slope of the CV-G_g curve at low G_g. These results indicate that localizing sufficient NaChs to JM is required to maintain CV when G_g is highly reduced.

In the cleft model with $100\%g_{Na,JM}$ and $0\%g_{Na,LM}$, the CV for normal G_g was no more than a half of that in the noncleft model. Adding NaChs to the LM increased the CV under normal G_g. By increasing the NaChs to $50\%g_{Na,LM}$, the CV came close to the physiological range in the longitudinal direction of ventricular myofiber (50–60 cm/s). A reduction in G_g under the condition with $100\%g_{Na,JM}$ and $50\%g_{Na,LM}$ also resulted in decreased CV, but an abrupt reduction in CV was observed when G_g was highly reduced (black and purple lines, Fig. 5 B). In the case of the abrupt reduction in CV, we observed the alternating pattern of long and short conduction delays (Fig. 5, C–E), suggesting the gap-junctional mechanism with the periodic and intermittent dysfunction of the EF mechanism contributed to this phenomenon.

To understand the mechanism of the slowing of AP propagation, how the reduced G_g influences the cleft potential between adjacent cells should be clarified. The amplitude of the gap-junctional current (I_g) reduced monotonically as the G_g decreased (Fig. S3 A). In the cases of $100\%g_{Na,JM}$ with $0–10\%g_{Na,LM}$ in the cleft model (red and blue lines in Fig. S3 B), the minimal value of the cleft potential (V_j) shifted more negatively as the G_g decreased. We confirmed in this study that such the marked negative cleft potential resulted in the activation of NaChs of the post-JM and thus resulted in the prevention of significant conduction delay (CV was kept at ~15 cm/s, as shown in Fig. 5 B) due to the EF mechanism. In contrast, when the NaCh in LM sufficiently increased ($\geq 30\%g_{Na,LM}$), the cleft potential showed a significant increase under the condition of low G_g (see black and purple lines in Fig. S3 B) (this mechanism is also discussed in the Supporting Material). Such high cleft potential caused the reduction of the NaCh current in the post-JM (see black and purple lines in Fig. S3 C) and the slow depolarization of the cell membrane (see asterisks in Fig. 5, D and E), resulting in the slowing of AP propagation.

Finally, we additionally conducted similar simulations with larger cell size ($22\sqrt{2}$ μm in width and $100\sqrt{2}$ μm in length), of which surface membrane area was twice that of the control cell. Then we found in the noncleft model with $100\%g_{Na,JM}$ and $0\%g_{Na,LM}$ that the larger cell size led to the increase in CV (compare the dashed line and the solid line in Fig. 6 A). In contrast, the CV in the cleft model with $100\%g_{Na,JM}$ and $0\%g_{Na,LM}$ was reduced by the increase in the cell size because the AP propagation via EF mechanism was markedly influenced by the subcellular NaCh distribution (Fig. 6 B). However, by adding the NaChs to the LM in the cleft model with $100\%g_{Na,JM}$ and $50\%g_{Na,LM}$ (Fig. 6 C), the relationship between the CV and the cell size
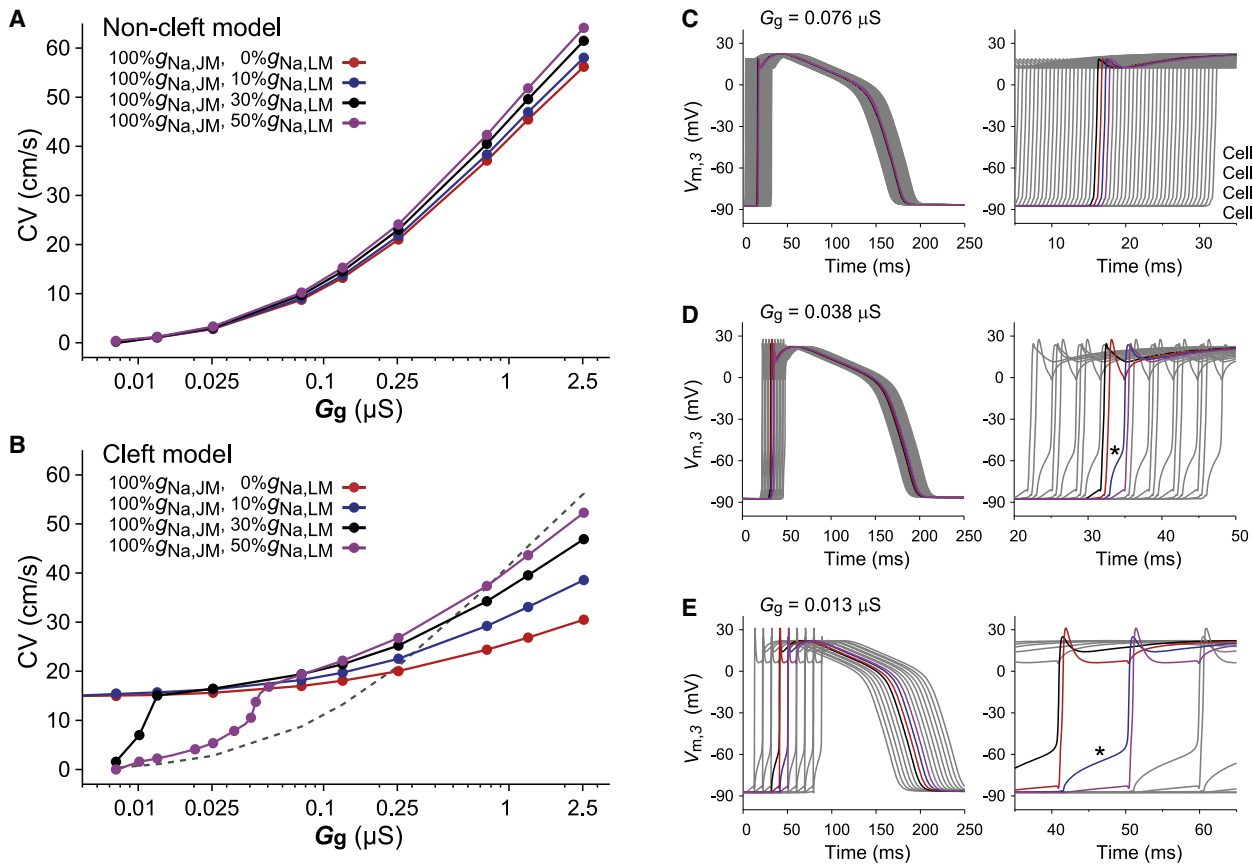
FIGURE 5 Conduction velocity (CV) as a function of gap-junctional conductance (G_g) in the noncleft (A) and cleft (B) strand models and change in qualitative properties of AP propagation observed in the case of $100\%g_{Na,JM}$ with $50\%g_{Na,LM}$ in the cleft model when the gap-junctional conductance (G_g) is decreased (C–E). For comparison, the dashed line in panel B represents the CV in the case of $100\%g_{Na,JM}$ with $0\%g_{Na,LM}$ in the noncleft model (*red line* in panel A). (C–E) The AP waveforms (*left*) and the enlarged diagrams at the phase-0 of APs (*right*), respectively. In the cleft model, we fixed the cleft conductance (G_j) at 0.25 μS, corresponding to the cleft width of 15 nm.

was quite similar to that in the noncleft model (compare to Fig. 6 A).

DISCUSSION

A number of theoretical studies previously investigated the nature of AP propagation in myofiber. For example, Sperelakis and co-workers (18,19) proposed the EF mechanism as a mechanism of AP propagation without gap-junctional coupling, and they demonstrated that the AP could propagate from cell to cell via the EF mechanism alone. Kucera et al. (24) raised the possibility that when NaChs were localized at JM, the EF mechanism contributes to AP propagation together with gap-junctional mechanism. Mori et al.
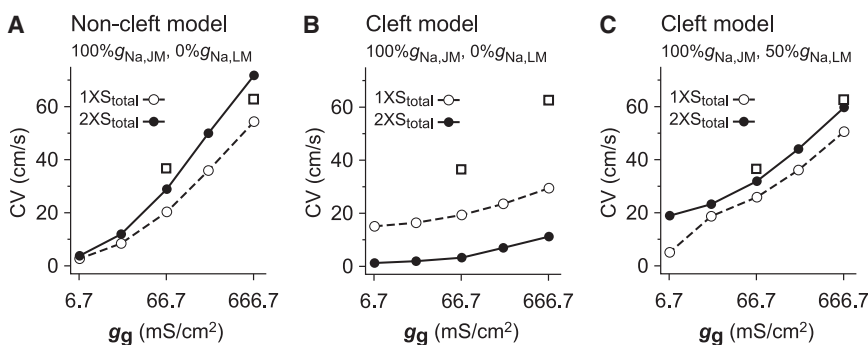

FIGURE 6 Effect of cell size on conduction velocity (CV) in the noncleft (A) and cleft (B and C) myofiber models. CV as a function of gap junctional conductance (g_g) in the noncleft (A) and cleft (B) models with $100\%g_{Na,JM}$ and $0\%g_{Na,LM}$, and in the cleft model (C) with $100\%g_{Na,JM}$ and $50\%g_{Na,LM}$. (*Dashed* and *solid lines*) g_g-CV relationship curve in the normal cell size case (100 μm in length and 22 μm in width) and that in the larger cell size case ($100\sqrt{2}$ μm in length and $22\sqrt{2}$ μm in width), respectively. In the larger cell, the total surface membrane area in a cell, S_{total}, was twice that of the normal cell. In this simulation, we assumed that the g_g at the JM in the larger cell was equal to that in the normal cell. For purpose of comparison, experimental data (16) are plotted as open squares on panels A–C.

(33) evaluated the effect of the intercellular cleft conductance on CV.

These theoretical studies mainly focused on the microstructural characteristics of intercellular cleft in the myofiber, and on the role of EF mechanism under physiological condition. On the other hand, our objective of this study was to clarify the roles of the subcellular NaCh distribution in AP propagation. In particular, we focused on the role of NaChs of the LM in AP propagation under the existence of EF mechanism. Then we found that the NaChs in the LM were responsible for both increasing CV and ensuring the robustness of AP propagation under conditions of low gap-junctional coupling. Based on these results, we concluded that the NaChs in the LM might be important for the homeostatic excitation propagation in both the physiological and pathological conditions.

AP propagation based on EF mechanism

To elucidate whether AP propagation depends only on the gap-junctional mechanism (Fig. 1 C), we first investigated the relationship between the subcellular NaCh distribution and the CV. Fig. 3 A demonstrates that the CV in the noncleft model is only determined by the total number of NaChs per cell independent of the number of NaChs expressed in LM. Spach et al. (25) also numerically confirmed that the alteration of subcellular NaCh distribution had no significant effect on the CV. However, in this study, when we incorporated the detailed microstructures of myofiber (such as cleft between cells and intercalated disk) into the model (Fig. 1 B), the subcellular NaCh distribution had surprising effects on AP propagation. The roles of such microstructures on AP propagation can be explained by the EF mechanism (18,19), together with the gap-junctional mechanism.

Subcellular NaCh distribution and AP waveform

The subcellular NaCh distribution in the cleft model altered the AP waveform (Figs. 2 and 4). When all NaChs were localized to JM, the AP waveform differed from the typically observed one in the ventricular epicardial single myocyte (34,35). The reason for this might be explained as follows. The alteration of the cleft potential based on the EF mechanism gave rise to the decrease in the driving force of the NaCh current in the post-JM (24). The decrease in the potential difference between the pre- and post-JMs due to the simultaneous supra-threshold depolarization of their JMs (see Fig. S1 A) reduced the current flowing through the gap junction. The intracellular axial current, consisting of both the gap-junctional current and the inward NaCh current in the post-JM, commonly depolarizes the local membrane (i.e., the LM segments) and generates an axial current to act on the pre-JM of the adjacent cell. Therefore, the intracellular axial current was reduced and this could not provide sufficient current to depolarize the adjacent cell.

Another reason for the reduction in the intracellular axial current is the high cleft resistance, resulting from the extremely narrow clefts. Such high cleft resistance induced the large negative extracellular potential and at the same time prevented the influx of NaCh current from the extracellular cleft space. Therefore, the phase-0 amplitude in AP decreased (Figs. 2 B and 4 A, right). On the other hand, the inward NaCh current at the LM boosted the local current and increased the intracellular axial current, causing the sufficient depolarization of the LM. Thereby, the normal AP in ventricular myocyte was formed (Figs. 2 C and 4 B, right).

Modulation of AP propagation by subcellular NaCh distribution

A previous experimental study (36) reported that the CV in the *Scn5a* heterozygous young mice, of which NaCh conductance was 50% of the control value (37), led to the decrease in CV by 16.9% (from 36.2 to 30.1 cm/s). As shown in Fig. 3 A, the half-NaCh conductance (50% $g_{Na,JM+LM}$) in the noncleft model caused the decrease in CV by 23.4% (from 54.3 to 41.6 cm/s), of which value was much larger than that in the experimental study (36). Such discrepancy between the experimental and simulation studies can be reduced by the use of the cleft model, which can reproduce the realistic AP propagation through both the gap-junctional and EF mechanisms. As shown in Fig. 3 B, when 10% of the g_{Na} was expressed at LM, the half-NaCh conductance resulted in the decrease in CV by 17.2% (from 37.7 to 31.2 cm/s), corresponding to the aforementioned experimental data (36).

The changes in CV in response to G_g suggest that the NaChs located at JM and LM play different roles in the modulation of CV. As shown in Fig. 5, A and B, the CV in the cleft model was less sensitive to G_g than in the noncleft model. Furthermore, we found that the addition of NaChs to LM increased the sensitivity of the CV to G_g in the cleft model. To confirm whether this characteristic response resulted from the increase in total NaCh number or the change in NaCh distribution itself, we conducted additional simulations, Fig. S2, and found that the tendency was essentially the same as Fig. 5 B. Therefore, we can conclude that the NaChs in LM compensate for the slowing CV by a decrease in G_g via the EF mechanism. Comparing with Fig. 5 B and Fig. S2, we additionally found that this compensation was stronger when the NaChs were abundant in JM (intercalated disk). This result was in agreement with the simulation results obtained by Kucera et al. (24).

Our results may explain the reduced CV in Cx43 CKO mice. Because the G_g in Cx43 CKO mice is decreased to <10% of the G_g in wild-type (17), the CV is expected to be approximately one-third of the wild-type, according to the cable theory (38). However, the actual CV measured by Gutstein et al. (16) was approximately half of that of

wild-type within either the longitudinal or the transversal directions of the myofiber. In fact, in this study, the CV was decreased to approximately one-half and approximately one-third of the control value in the cleft and noncleft models, respectively (Fig. 5 B). Therefore, in an actual myocardial tissue, the EF mechanism could serve to prevent the reduction of the CV by the decrease in G_g.

If all NaChs locating in JM is the case, the CV would be kept at 15 cm/s even without gap-junctional current, i.e., $G_g = 0$ μS (Fig. 5 B). However, Beauchamp et al. (39) demonstrated that the conduction block occurred by both the knockout of Cx43 and the pharmacological block of Cx45, and they concluded that the EF mechanism does not contribute to the mechanism of AP propagation. As shown in this simulation study, when sufficient NaChs are expressed in LM (>30%g$_{Na,LM}$) in the cleft model, the contribution of EF mechanism decreased due to a reduction of the cleft potential amplitude (Fig. S3 B) and thus the conduction block could be reproduced (*black* and *purple lines* in Fig. 5 B). Therefore, the results of our study suggest the possibility, without conflicting with Beauchamp et al. (39), that the EF mechanism can contribute to the AP propagation.

Effect of cell size on AP propagation

Previous studies (25,40–42) have shown that AP propagation in cardiac tissues under the physiological and/or pathophysiological conditions was highly influenced by both size and shape of the myocardial cells. As shown in Fig. 6 B, the localization of NaCh to the JM in the cleft model led to an inverse effect of the increase in cell size on the CV in contrast with the noncleft model. This is due to both the reduction in the number of NaChs of JM and the reduction in LM excitability. However, in the same cleft model but with the addition of NaChs to LM, the CV in the myofiber composed of larger cells was higher than that in the case of normal cell size (Fig. 6 C). This result further supports our finding that the presence of NaChs in LM plays an important role in the AP propagation. Nevertheless, further studies will be required because the effect of the cell size on AP propagation in the cleft model is far more complicated than that in the noncleft model.

Limitations of the model

In addition to the localization of NaCh to the JM, other ion channel and transporter proteins are also distributed in the JM, such as voltage-gated K+ channels (43,44), Na$^+$ pump (Na$^+$/K$^+$-ATPase) (45), and Na$^+$-Ca^{2+} exchanger (46). However, we did not take into account the localization of their ion channels and transporters to the JM. Such ion channels and transporters might have some effects on CV via the change of ion concentration in the intercellular cleft space (33).

Physiological implications

The existence of NaCh at LM was experimentally confirmed by several studies (20–23). However, the role of NaChs at LM is still controversial. Maier et al. (21) stated the possibility that the NaChs at transverse tubule (LM segment) make the myocyte more excitable, thereby strengthening the contraction via excitation-contraction coupling. On the other hand, Brette and Orchard (47) reported that NaChs at transverse tubule did not change the calcium transient and therefore the NaChs had no effect on excitation-contraction coupling. In this study, we found, to our knowledge, a novel role of NaChs at LM in increasing the robustness of the AP propagation. Our simulations clearly showed that the NaChs in the LM act as a booster for the intracellular axial current. Furthermore, in order for the EF mechanism (cleft model) to coexist with a normal prediction of the physiological AP waveform (compare Fig. 2, B and C), the existence of NaChs at LM is indispensable. From the point of view of CV, the NaChs at LM are necessary for the cleft model to reproduce the physiological CV at ~60 cm/s in the longitudinal direction of the myofiber.

Clinical implications

The APs with insufficient depolarization from phase-0 to phase-2 of the AP (Fig. 2 B) and with a marked abbreviation of the AP duration (Fig. 4 A, right) by the decrease of NaChs in the LM evoke the change of AP morphology commonly observed in patients with the Brugada syndrome (48,49). In fact, Mohler et al. (22) and Lowe et al. (50) have suggested the possibility that gene mutation in ankyrin-binding motif of the NaCh causing the decrease of NaChs at cell membrane in ventricular myocytes was associated with Brugada syndrome.

Furthermore, immunohistochemical staining by Baba et al. (23) revealed that NaChs of myocytes in the infarct-border zone are localized in intercalated disk (JM) rather than in LM, whereas those in the normal zone are homogeneously distributed throughout the entire cell membrane. Based on the results of this study, such inhomogeneous change in NaCh distribution (the decrease of NaChs in LM) could avoid conduction block at low G_g condition produced by ischemia (compare *purple line* and *red line* in Fig. 5 B), resulting in the homeostasis of AP propagation. This also implies that the NaCh blockade (class I antiarrhythmic drug) in the ischemic myocardium might cause conduction block (Fig. 3 B), leading to a more arrhythmogenic condition.

SUPPORTING MATERIAL

Additional methods with five equations, additional results, one table, and three figures are available at http://www.biophysj.org/biophysj/supplemental/S0006-3495(10)05262-8.

REFERENCES

1. Rüdisüli, A., and R. Weingart. 1989. Electrical properties of gap junction channels in guinea-pig ventricular cell pairs revealed by exposure to heptanol. *Pflugers Arch.* 415:12–21.

2. de Groot, J. R., T. Veenstra, …, E. E. Verheijck. 2003. Conduction slowing by the gap junctional uncoupler carbenoxolone. *Cardiovasc. Res.* 60:288–297.

3. Kléber, A. G., C. B. Riegger, and M. J. Janse. 1987. Electrical uncoupling and increase of extracellular resistance after induction of ischemia in isolated, arterially perfused rabbit papillary muscle. *Circ. Res.* 61:271–279.

4. Kieval, R. S., J. F. Spear, and E. N. Moore. 1992. Gap junctional conductance in ventricular myocyte pairs isolated from postischemic rabbit myocardium. *Circ. Res.* 71:127–136.

5. Hoyt, R. H., M. L. Cohen, and J. E. Saffitz. 1989. Distribution and three-dimensional structure of intercellular junctions in canine myocardium. *Circ. Res.* 64:563–574.

6. Smith, J. H., C. R. Green, …, N. J. Severs. 1991. Altered patterns of gap junction distribution in ischemic heart disease. An immunohistochemical study of human myocardium using laser scanning confocal microscopy. *Am. J. Pathol.* 139:801–821.

7. Yeager, M. 1998. Structure of cardiac gap junction intercellular channels. *J. Struct. Biol.* 121:231–245.

8. Cooklin, M., W. R. J. Wallis, …, C. H. Fry. 1997. Changes in cell-to-cell electrical coupling associated with left ventricular hypertrophy. *Circ. Res.* 80:765–771.

9. Poelzing, S., and D. S. Rosenbaum. 2004. Altered connexin43 expression produces arrhythmia substrate in heart failure. *Am. J. Physiol. Heart Circ. Physiol.* 287:H1762–H1770.

10. Spragg, D. D., F. G. Akar, …, D. A. Kass. 2005. Abnormal conduction and repolarization in late-activated myocardium of dyssynchronously contracting hearts. *Cardiovasc. Res.* 67:77–86.

11. Spach, M. S., W. T. Miller, 3rd, …, E. A. Johnson. 1981. The discontinuous nature of propagation in normal canine cardiac muscle. Evidence for recurrent discontinuities of intracellular resistance that affect the membrane currents. *Circ. Res.* 48:39–54.

12. Rudy, Y., and W. L. Quan. 1987. A model study of the effects of the discrete cellular structure on electrical propagation in cardiac tissue. *Circ. Res.* 61:815–823.

13. Shaw, R. M., and Y. Rudy. 1997. Ionic mechanisms of propagation in cardiac tissue. Roles of the sodium and L-type calcium currents during reduced excitability and decreased gap junction coupling. *Circ. Res.* 81:727–741.

14. Ya, J., E. B. Erdtsieck-Ernste, …, W. H. Lamers. 1998. Heart defects in connexin43-deficient mice. *Circ. Res.* 82:360–366.

15. Morley, G. E., D. Vaidya, …, J. Jalife. 1999. Characterization of conduction in the ventricles of normal and heterozygous Cx43 knockout mice using optical mapping. *J. Cardiovasc. Electrophysiol.* 10:1361–1375.

16. Gutstein, D. E., G. E. Morley, …, G. I. Fishman. 2001. Conduction slowing and sudden arrhythmic death in mice with cardiac-restricted inactivation of connexin43. *Circ. Res.* 88:333–339.

17. Yao, J. A., D. E. Gutstein, …, A. L. Wit. 2003. Cell coupling between ventricular myocyte pairs from connexin43-deficient murine hearts. *Circ. Res.* 93:736–743.

18. Sperelakis, N., and J. E. Mann, Jr. 1977. Evaluation of electric field changes in the cleft between excitable cells. *J. Theor. Biol.* 64:71–96.

19. Sperelakis, N., and K. McConnell. 2002. Electric field interactions between closely abutting excitable cells. *IEEE Eng. Med. Biol. Mag.* 21:77–89.

20. Cohen, S. A. 1996. Immunocytochemical localization of rH1 sodium channel in adult rat heart atria and ventricle. Presence in terminal intercalated disks. *Circulation.* 94:3083–3086.

21. Maier, S. K. G., R. E. Westenbroek, …, W. A. Catterall. 2002. An unexpected role for brain-type sodium channels in coupling of cell surface depolarization to contraction in the heart. *Proc. Natl. Acad. Sci. USA.* 99:4073–4078.

22. Mohler, P. J., I. Rivolta, …, V. Bennett. 2004. Na$_v$1.5 E1053K mutation causing Brugada syndrome blocks binding to ankyrin-G and expression of Na$_v$1.5 on the surface of cardiomyocytes. *Proc. Natl. Acad. Sci. USA.* 101:17533–17538.

23. Baba, S., W. Dun, …, P. A. Boyden. 2005. Remodeling in cells from different regions of the reentrant circuit during ventricular tachycardia. *Circulation.* 112:2386–2396.

24. Kucera, J. P., S. Rohr, and Y. Rudy. 2002. Localization of sodium channels in intercalated disks modulates cardiac conduction. *Circ. Res.* 91:1176–1182.

25. Spach, M. S., J. F. Heidlage, …, R. C. Barr. 2000. Electrophysiological effects of remodeling cardiac gap junctions and cell size: experimental and model studies of normal cardiac growth. *Circ. Res.* 86:302–311.

26. Severs, N. J. 1995. Cardiac muscle cell interaction: from microanatomy to the molecular make-up of the gap junction. *Histol. Histopathol.* 10:481–501.

27. Katz, B. 1966. Nerve, Muscle and Synapse. McGraw-Hill, New York.

28. Suzuki, S., S. Murakami, …, Y. Kurachi. 2008. In silico risk assessment for drug-induction of cardiac arrhythmia. *Prog. Biophys. Mol. Biol.* 98:52–60.

29. Findlay, I., S. Suzuki, …, Y. Kurachi. 2008. Physiological modulation of voltage-dependent inactivation in the cardiac muscle L-type calcium channel: a modeling study. *Prog. Biophys. Mol. Biol.* 96:482–498.

30. Luo, C. H., and Y. Rudy. 1994. A dynamic model of the cardiac ventricular action potential. I. Simulations of ionic currents and concentration changes. *Circ. Res.* 74:1071–1096.

31. Faber, G. M., and Y. Rudy. 2000. Action potential and contractility changes in [Na$^+$]$_i$ overloaded cardiac myocytes: a simulation study. *Biophys. J.* 78:2392–2404.

32. Aiba, T., W. Shimizu, …, K. Sunagawa. 2005. Cellular and ionic mechanism for drug-induced long QT syndrome and effectiveness of verapamil. *J. Am. Coll. Cardiol.* 45:300–307.

33. Mori, Y., G. I. Fishman, and C. S. Peskin. 2008. Ephaptic conduction in a cardiac strand model with 3D electrodiffusion. *Proc. Natl. Acad. Sci. USA.* 105:6463–6468.

34. Osaka, T., I. Kodama, …, K. Yamada. 1987. Effects of activation sequence and anisotropic cellular geometry on the repolarization phase of action potential of dog ventricular muscles. *Circulation.* 76:226–236.

35. Aiba, T., W. Shimizu, …, K. Sunagawa. 2003. Transmural heterogeneity of the action potential configuration in the feline left ventricle. *Circ. J.* 67:449–454.

36. van Veen, T. A. B., M. Stein, …, H. V. van Rijen. 2005. Impaired impulse propagation in Scn5a-knockout mice: combined contribution of excitability, connexin expression, and tissue architecture in relation to aging. *Circulation.* 112:1927–1935.

37. Papadatos, G. A., P. M. R. Wallerstein, …, A. A. Grace. 2002. Slowed conduction and ventricular tachycardia after targeted disruption of the cardiac sodium channel gene Scn5a. *Proc. Natl. Acad. Sci. USA.* 99:6210–6215.

38. Arnsdorf, M. F., and J. C. Makielski. 2001. Excitability and impulse propagation. *In* Heart Physiology and Pathophysiology, 4th Ed. Y. Kurachi, A. Terzic, M. V. Cohen, and N. Sperelakis, editors. California Academic Press, Millbrae, CA. 99–132.

39. Beauchamp, P., C. Choby, …, A. G. Kléber. 2004. Electrical propagation in synthetic ventricular myocyte strands from germline connexin43 knockout mice. *Circ. Res.* 95:170–178.

40. Joyner, R. W. 1982. Effects of the discrete pattern of electrical coupling on propagation through an electrical syncytium. *Circ. Res.* 50:192–200.

41. Kucera, J. P., and Y. Rudy. 2001. Mechanistic insights into very slow conduction in branching cardiac tissue: a model study. *Circ. Res.* 89:799–806.

42. Satoh, H., L. M. D. Delbridge, …, D. M. Bers. 1996. Surface/volume relationship in cardiac myocytes studied with confocal microscopy and membrane capacitance measurements: species-dependence and developmental effects. *Biophys. J.* 70:1494–1504.

43. Barry, D. M., J. S. Trimmer, …, J. M. Nerbonne. 1995. Differential expression of voltage-gated K$^+$ channel subunits in adult rat heart. Relation to functional K$^+$ channels? *Circ. Res.* 77:361–369.

44. Mays, D. J., J. M. Foose, …, M. M. Tamkun. 1995. Localization of the Kv1.5 K$^+$ channel protein in explanted cardiac tissue. *J. Clin. Invest.* 96:282–292.

45. McDonough, A. A., Y. Zhang, …, J. S. Frank. 1996. Subcellular distribution of sodium pump isoform subunits in mammalian cardiac myocytes. *Am. J. Physiol.* 270:C1221–C1227.

46. Kieval, R. S., R. J. Bloch, …, W. J. Lederer. 1992. Immunofluorescence localization of the Na-Ca exchanger in heart cells. *Am. J. Physiol.* 263:C545–C550.

47. Brette, F., and C. H. Orchard. 2006. No apparent requirement for neuronal sodium channels in excitation-contraction coupling in rat ventricular myocytes. *Circ. Res.* 98:667–674.

48. Brugada, P., and J. Brugada. 1992. Right bundle branch block, persistent ST segment elevation and sudden cardiac death: a distinct clinical and electrocardiographic syndrome. A multicenter report. *J. Am. Coll. Cardiol.* 20:1391–1396.

49. Kurita, T., W. Shimizu, …, Y. Kosakai. 2002. The electrophysiologic mechanism of ST-segment elevation in Brugada syndrome. *J. Am. Coll. Cardiol.* 40:330–334.

50. Lowe, J. S., O. Palygin, …, P. J. Mohler. 2008. Voltage-gated Na$_v$ channel targeting in the heart requires an ankyrin-G dependent cellular pathway. *J. Cell Biol.* 180:173–186.